Measuring droplet size distributions from overlapping interferometric particle images

Measuring droplet size distributions from overlapping interferometric particle images

Humberto Bocanegra Evans, Nico Dam, Dennis van der Voort, Guus Bertens, and Willem van de Water'

Citation: Rev. Sci. Instrum. **86**, 023709 (2015); doi: 10.1063/1.4909537
View online: http://dx.doi.org/10.1063/1.4909537
View Table of Contents: http://aip.scitation.org/toc/rsi/86/2
Published by the American Institute of Physics

Measuring droplet size distributions from overlapping interferometric particle images

Humberto Bocanegra Evans,[1] Nico Dam,[2] Dennis van der Voort,[1] Guus Bertens,[1] and Willem van de Water[1,a)]
[1]*Faculty of Applied Physics, Technische Universiteit Eindhoven, Eindhoven, The Netherlands*
[2]*Faculty of Mechanical Engineering, Technische Universiteit Eindhoven, Eindhoven, The Netherlands*

(Received 22 January 2015; accepted 8 February 2015; published online 24 February 2015)

Interferometric particle imaging provides a simple way to measure the probability density function (PDF) of droplet sizes from out-focus images. The optical setup is straightforward, but the interpretation of the data is a problem when particle images overlap. We propose a new way to analyze the images. The emphasis is not on a precise identification of droplets, but on obtaining a good estimate of the PDF of droplet sizes in the case of overlapping particle images. The algorithm is tested using synthetic and experimental data. We next use these methods to measure the PDF of droplet sizes produced by spinning disk aerosol generators. The mean primary droplet diameter agrees with predictions from the literature, but we find a broad distribution of satellite droplet sizes. © *2015 AIP Publishing LLC*. [http://dx.doi.org/10.1063/1.4909537]

I. INTRODUCTION

Optical techniques for measuring the size of small droplets are used in fields as diverse as spray combustion and droplet dynamics in turbulent clouds. Known techniques are phase-Doppler anemometry, which provides a simultaneous measurement of the droplet size and velocity at a single point in space, and interferometric particle imaging (IPI). The latter provides droplet sizes in a plane and is quite attractive because of its extremely simple setup.

Briefly, when droplets are illuminated by coherent light, an interference pattern results from rays passing over and through the droplet. These interference patterns are made visible by out-of-focus imaging of the droplets: each droplet corresponds to a disk in the image plane whose diameter is determined by the lens aperture. The disk image is modulated by fringes whose spacing is inversely proportional to the droplet diameter. The optical setup, therefore, merely needs a laser sheet and a camera. It is not straightforward, however, how to interpret the images in order to obtain a dependable estimate of the droplet size distribution. The main problem is the overlap of particle images in dense sprays. The purpose of the present paper is to contribute a new way to analyze IPI images, especially those that have many particle overlaps.

An extensive literature exists on IPI, and points of concern have been the avoidance of particle disk overlaps, methods to identify droplet disks in images, and methods to find the spatial frequency of interference fringes inside the particle disks. In all previous works, particle disk overlaps were considered detrimental for further analysis. A careful statistical analysis of the chances of overlaps, given the particle density in images and the details of the optical arrangement, was provided by Damaschke, Nobach, and Tropea.[1] The degree of disk overlap was quantified by the overlap coefficient γ, which is the ratio of the overlap area to the total area covered by particle disks. It was speculated that a value $\gamma = 0.1$ should still be tolerable.

The chances of overlaps occurring can be reduced by using cylindrical lenses or masks so that particle images are compressed in the direction parallel to the fringes.[2] This technique has been refined in a recent paper by Hardalupas *et al.*,[3] who used a rectangular mask and a cylindrical lens, resulting in narrow, rectangular interference patterns. Although these lines contain the pertinent information for droplet sizing, their identification in images is more difficult than that of circular disks. By using two optical channels, both the positions and velocities could be measured in dilute droplet concentrations.

Droplet size probability distribution function (PDF's) using interferometric particle imaging were measured by Glover, Skippon, and Boyle[4] using the Hough transform to find particle disks and a least-squares fit to find the spatial fringe frequency. Overlapping images were discarded. The accuracy of the Fourier transform to determine the fringe frequency in the presence of noise was discussed by Dehaeck and Beeck.[5]

The purpose of the present paper is to present a novel algorithm for the analysis of the images obtained, with the purpose of extracting a good estimate of the PDF of particle sizes in the presence of particle-disk overlaps. The key question is how much overlap is allowed before the PDF becomes inaccurate. Therefore, it is not our purpose to correctly identify all droplets, and in fact, we will only find a fraction of all droplets in cluttered images.

The wavelet approach of Hardalupas *et al.*[3] has inspired the current paper. As the size and shape of the particle disks is known *a priori*, we will use a correlation technique to locate the particle disks in an image. These candidate disks will be organized *hierarchically*, which is a key step in tackling the overlap problem. Then, we will use a Fourier transform to arrive at a first estimate of the wavelength and phase of the interference pattern inside disks. Next, this estimate is refined

a)Electronic mail: w.v.d.water@tue.nl

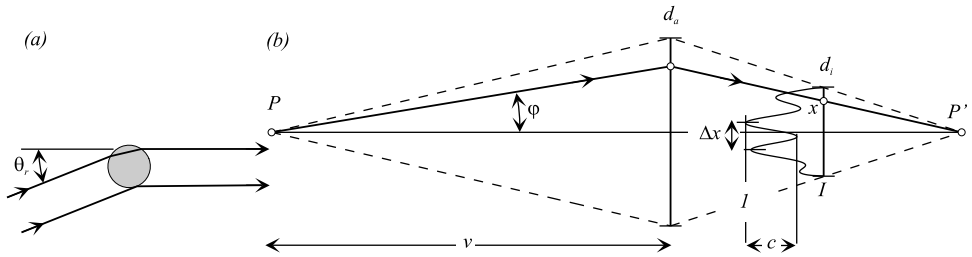

FIG. 1. (a) Geometric arrangement of interferometric particle imaging. (b) Schematic of the optical arrangement of IPI for a droplet positioned at the optical axis. The point P represents the position of the particle, v is the object distance, φ is an angular coordinate, with $\Delta\varphi$ (Eq. (1)) the angular fringe separation, while Δx is its linear counterpart. The focused image plane lies at point P'. The interference pattern has spot diameter d_i, and the aperture diameter is d_a. If the maximum intensity in the fringes is 1, c determines the fringe contrast.

using a least-squares fit of the intensity profile of a fringe pattern.

A similar two-step approach was followed by Bilsky, Lozhkin, and Markovich;[6] the overlap problem was tackled by a rejection procedure based on fringe contrast, signal to noise ratio, and consistency between droplet size and luminance. In addition, they discuss the validity of the geometrical approach (Eq. (2)) in relation to the full Mie scattering problem. In contrast, our only selection criterion is a recognizable local maximum of the convolution between the image and the used disk-like kernel. In a recent paper,[7] fringe frequencies were determined precisely using Fourier- and interpolation techniques.

Compression of the disks to ellipses through cylindrical optics is an excellent scheme to lessen the detrimental effect of overlaps, but it comes at the expense of a loss of information. We will demonstrate that the algorithms described here work for elliptical particle disks at any aspect ratio, but we will restrict ourselves to circular disks and ordinary optics in the experiments. Clearly, accurate PDF's at larger droplet concentrations are accessible through usage of cylindrical optics, but it is not a fundamental extension of our results.

We will test our method using simulated images, and experiments on calibrated micron-sized glass spheres. We will further illustrate our methods by measuring the PDF of droplets generated by a spinning disk aerosol generator at various rotation rates. We compare the mean of the droplet size to the predicted one, show the PDF of droplet sizes, and discuss the origin of the measured size distribution, which is not documented well in the literature. We also measure the droplet sizes using a commercial apparatus (Malvern Mastersizer), the results of which are in excellent agreement with those of our simple IPI setup and analysis.

II. INTERFEROMETRIC PARTICLE IMAGING

Interferometric particle imaging, first proposed by König, Anders, and Frohn[8] and Ragucci, Cavaliere, and Massoli,[9] presents particularly convenient characteristics when compared to other methods: it has the capability of yielding two-dimensional data while most other available methods are point measurements. Additionally, the only necessary equipment is a reasonably coherent light source and a camera. In cases where droplets have relatively high velocities, the use of a pulsed light source is required to "freeze" the particles.

The scattering of coherent light off a droplet results from interference between light wavefronts passing over and through the droplet. However, for droplets larger than the wavelength of light, the picture can be simplified to rays originating from two glare points, one corresponding to a reflected ray, and one to a ray which is refracted twice. A derivation of the difference in optical path lengths of these two rays can be found in Albrecht *et al.*[10]

The geometric arrangement of IPI is sketched in Fig. 1(a). The angular separation $\Delta\varphi$ of the fringes is determined by the optical path length difference of the two scattered rays,

$$\Delta\varphi = \frac{2\lambda}{\mathrm{A}(\theta_r) d_p}, \tag{1}$$

with d_p, the particle diameter and λ, the wavelength of the incident light. The factor $\mathrm{A}(\theta_r)$ reflects the geometry of the two rays passing through and over the droplet,

$$\mathrm{A}(\theta_r) = \left(m\cos(\theta_r/2) + \frac{m\sin(\theta_r/2)}{\sqrt{m^2+1-2m\cos(\theta_r/2)}} \right). \tag{2}$$

The scattering angle between the optical axis of the system and the incident light is θ_r, and m is the relative refractive index. If the two rays have equal intensity, the visibility of the fringes is maximal. In general, the contrast depends on the scattering angle θ_r, the refractive index m, and the polarization of the light. For water droplets with a diameter $d_p \simeq 20\ \mu$m, the optimal angles are approximately $\theta_r = 95°$ and $\theta_r = 70°$ for parallel and perpendicular polarizations, respectively.

Angular information of scattered light is obtained from out-of-focus imaging, with the optical arrangement sketched in Fig. 1(b). In this arrangement, particle images are circular disks with diameter d_i determined by the location of the object plane and the size d_a of the lens aperture. The intensity in the spots is modulated by fringes.

If x is an image coordinate, the fringe spacing Δx is $\Delta x = (d_i/d_a) v\ \Delta\varphi$. Since x and d_i can be measured in pixels, the only additional information needed is the size d_a of the lens aperture and the object distance v. Roughly, the particle size is proportional to the number of fringes observed in a droplet image. Counting fringes provides the droplet sizes on a discrete scale. However, in this paper, we will use the detailed intensity information, which, in principle, allows us to quantify the size of particles that produce less than two fringes. Nevertheless, particle size measurements benefit from large spatial fringe frequencies.

In order to have many fringes in a particle image, v must be small and d_a must be large. As the size of the out-focus images is determined by the lens aperture, dense droplet clouds lead to many overlapping particle disks. The question is how much particle overlap can we tolerate before the particle size PDF is affected significantly?

The sphericity of the droplets and particles can also affect the accuracy of the results. Dehaeck and Beeck[5] looked at the influence of bubble deformation on their size determination, and discussed other sources of error such as the tilt angle of the deformed droplet and the uncertainty arising from the angle θ_r and the refractive index m. In our particle size range, however, we do not expect particle deformation since the droplets are much smaller than any length scale of the flow, and their velocities within the measurement volume are relatively low.

A. Image processing

The purpose of the image analysis is to locate the particle images, determine the spatial frequency of the fringes within each particle image, and make a histogram of particle sizes from the measured spatial frequencies. For brevity of the exposition, we assume in the sequel that particle images are circular disks with diameter d_i. However, the same arguments hold for ellipses, with a trivial adaptation of the formulae. The steps of the analysis are illustrated in Fig. 2.

The first task is locating the particle disks in images. We make use of the circumstance that, when droplets are illuminated by a thin light sheet and the optical axis is perpendicular to the incident light sheet (as in our case), all particle images have the same diameter d_i, and we convolve the image with a kernel $\kappa(x, y) = 1$ if $x^2 + y^2 < (d_i/2)^2$, and 0 otherwise. For off-axis imaging, i.e., θ_r different from 90°, droplet images have different diameters. This, however, can be corrected by meeting the Scheimpflug condition.

Next, we seek for the local maxima in the convolved image, we do that in the following hierarchical manner. A center pixel (x_0, y_0) is a local maximum if its intensity is a factor F larger than all points on the circle $(x - x_0)^2 + (y - y_0)^2 = (d_i/2)^2$. For F, we typically took the value $F = 1.1$. This leaves us with many candidate centers in the image. These are further pruned by sorting their intensities in decreasing order, picking the first candidate center, and deleting all other candidate centers that fall within the search circle of this particular disk, and so on. For isolated particle images, this procedure leaves us with a complete list of particle images that satisfy the intensity contrast criterion. Exactly the same steps can be used for ellipsoidal particle images with circles replaced by ellipsoids. This is the distinguishing step of our method: we identify candidate particle disks in a hierarchical fashion. We will demonstrate that most of the time this new approach indeed finds the clearest one in a group of overlapping particle disks.

After finding the particle images, the pixel values are summed along the fringe orientation (y-direction), resulting in an intensity distribution $I(x)$ for each of them. The function $I(x)$, $x \in [-d_i/2, d_i/2]$ is defined at discrete pixel locations x_i; it is differentiated to reduce the pedestal modulation, extended with zeros to the left $x < -d_i/2$, and to the right, $x > d_i/2$, and Fourier transformed. The zero padding provides an interpolation on the spatial frequencies. A typical energy spectrum is shown in Fig. 2(d).

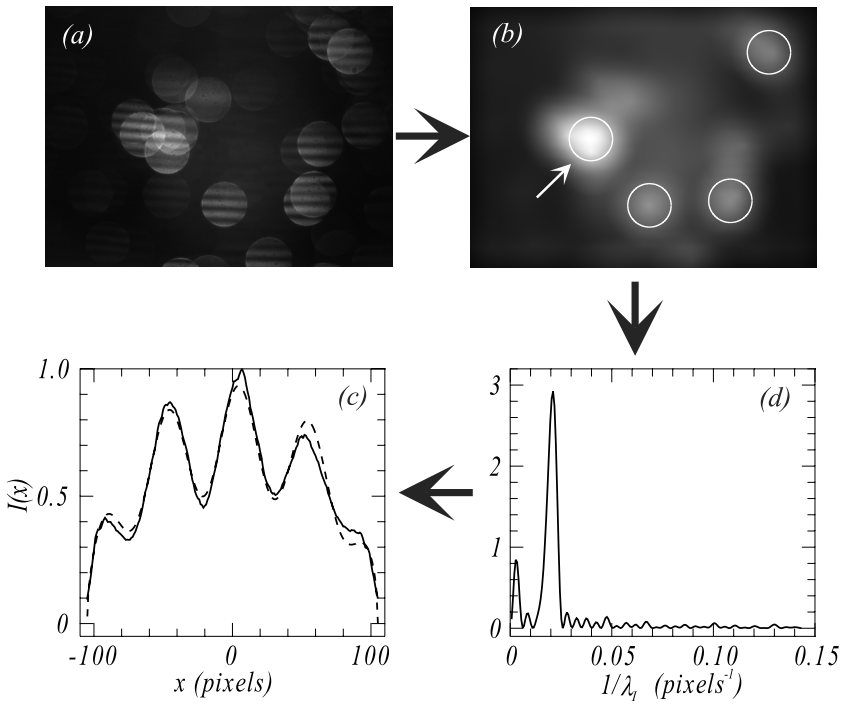

FIG. 2. The steps of the used procedure. The droplets are generated by a spinning disk aerosol generator, with disk radius $R = 1$ cm and angular velocity $\omega = 2.2 \times 10^3\,\mathrm{s}^1$. The original image is in (a) and the result after convolution with a disk-like kernel is shown in (b). The circles show the guessed particle images. An energy spectrum of the fringes in one of these particle disks is shown in (d). The location of the peak and the phase at the peak wavenumber are used for a fit of the intensity. Full line in (c) is the measured intensity profile $I(x)$, dashed line is a fit. The fitted spatial frequency is a direct measure for the droplet diameter. The white arrow points to a spot where several disks overlap. This particle image leads to a wavelength which equals the particle image diameter.

From the Fourier transform, we determine the spatial wavelength λ_I of the maximum energy, and the corresponding phase ϕ. As Fig. 2(d) illustrates, the spectrum of an isolated particle disk comes with two peaks, one corresponding to the spatial fringe frequency and one corresponding to the droplet disk size. In case of severely overlapping disks, the latter peak dominates. These overlapping disks are ignored, similarly to droplet images with only fringe, or no fringes at all. Due to the optical arrangement in our experiment, and the rather small particle sizes, often no more than a few fringes are observed and further refinement of the found fringe wavelengths λ_I is necessary. To this aim, we fit the measured intensity function $I(x)$ to

$$I(x) = a\left[1 - \left(\frac{2x}{d_i}\right)^2\right]^{1/2} \frac{(1 + c\cos[2\pi(x/\lambda_I + \phi)])}{(1 + c)}, \quad (3)$$

where the intensity a, the fringe contrast c, λ_I, and the phase ϕ are determined in a least-squares procedure. The first factor results from the compression of the particle image in the y-direction and the second factor represents the fringes. Since for λ_I and ϕ a good estimate already exists from the Fourier transform, the least squares procedure was restrained: the phase ϕ and wavelength λ_I were allowed to vary 50% around their initial Fourier estimate, while the amplitude $0.75 < a < 1.25$ and contrast $0.5 < c < 1$. Without the refinement provided by Eq. (3), the fringe wavelengths and thus measured particle sizes approximately lock to discrete values.

In summary, we locate particle disks using the convolution with a simple disk-like kernel which can be viewed as a single-scale wavelet transform. Without doubt this kernel can be further refined, for example, to emphasize edges. The convolution can be done efficiently using the Fourier transform. Next, we find the spatial fringe frequency through another Fourier transform, the result of which provides seeds for a least-squares fit of the fringe profile. We emphasize that the ingredients of this procedure are not new—both the Fourier-[11] and the wavelet transform have been discussed before[6,7]—but the combination, and especially the hierarchical approach to find the best particle disks is new.

The question now is how accurately this procedure finds particle size PDF's in the case of particle disk overlaps. We will first answer this question using simulated particle images.

B. Simulated particle images

Simulated particle images were made by randomly sprinkling disks with fixed diameter d_i and intensity profile

$$I(x, y) = \left[1 + \cos\left(\frac{2\pi x}{\Delta x}\right)\right] I_p(x - x_0, y - y_0), \quad (4)$$

where $I_p(x, y)$ is I_0 inside the disk $x^2 + y^2 \le d_i^2/4$, and 0 outside, and Δx is inversely proportional to the particle diameter d_p, $\Delta x = \mathrm{A}d_i/d_p$, with a proportionality factor A, whose value is characteristic for our experiments. In the experiments, the droplets are illuminated using a laser sheet with a Gaussian intensity distribution, accordingly the droplet intensity was taken proportional to $\exp(-z^2)$, with z sprinkled uniformly on the interval [-1.5, 1.5]. The particle diameters d_p were picked randomly from a Gaussian distribution,

$$P(d_p) = \frac{1}{d_\sigma \pi^{1/2}} \exp\left[-\frac{(d_p - d_m)^2}{d_\sigma^2}\right], \quad (5)$$

with mean d_m and Gaussian width d_σ.

We will test our methods for a PDF $P(d_p)$ with a single mean droplet diameter d_m and smallest droplets giving a single fringe only, and for a very broad PDF involving 3 mean diameters which are very different. It is for these cases that we expect particle overlaps to be most detrimental. We first simulate data over a range of droplet diameters $d_m = 10 \ldots 30$ μm, in steps of 2.5 μm and Gaussian width $d_\sigma = 5$ μm. This range was chosen because the smallest droplet diameters come with less than two fringes. Figs. 3(a) and 3(b) show the resulting distributions produced by the processing algorithm and compare them with the simulated distribution. It can be seen that our procedure correctly reproduces the prescribed $P(d_p)$, but that problems arise at small particle diameters, where a particle image contains a single fringe. As expected, this problem is aggravated when particle images clutter. In the case of Figs. 3(a) and 3(c), a found droplet disk overlaps on average with 2.5 disks in the simulated image, with an overlap coefficient $\gamma = 0.24$[1] and only a fraction 0.36 of the actually seeded droplets is found. For Figs. 3(b) and 3(d), a found disk overlaps with 1.6 simulated disks, $\gamma = 0.12$, and a fraction 0.55 of the simulated disks is found. Probability density functions for a very broad range of particle sizes are shown in Figs. 3(b) and 3(d), with the same total number of disks as in Figs. 3(a) and 3(c), respectively. The problem with overlaps now is that in a broad range of sizes, the number of small droplets, with few fringes per disk, is underestimated as overlaps introduce extra (but out-phase) fringes in a particle disk. Also shown are the results for 129 *ellipsoidal* particle images per frame with aspect ratio 1/2. These results coincide with those of 63 circular particle images per frame.

It may seem surprising that images with many overlapping particle disks, such as shown in Fig. 3(a) still result in relatively small errors in measured particle size PDF's. We will try to understand this by using the simulated images, in which all droplet intensities and locations are known *a priori*, for further statistical analysis.

The first simple question is what fraction of input-particle disks is found, and what the measured PDF is using a dense image. An answer is given for particles drawn from a Gaussian PDF (Eq. (5)) at increasing density. In Fig. 4, we show the ratio of the found disks over the total simulated number as a function of the overlap coefficient γ. It turns out that a maximum of approximately 25% of the image area can be identified as diffraction disks. As Fig. 4 illustrates, even for $\gamma = 0.51$, the error in the measured droplet size PDF is small.

A more subtle question is about relation between found particle disks and particles in the simulation. The problem of overlaps is that found image disks may not correspond to one particular droplet, but may be positioned somewhere in the overlap region and cover several different droplet images. The spatial fringe frequency would in that case not correspond to any of the overlapping particle images. The advantage of our disk location method is that it is strongly biased towards

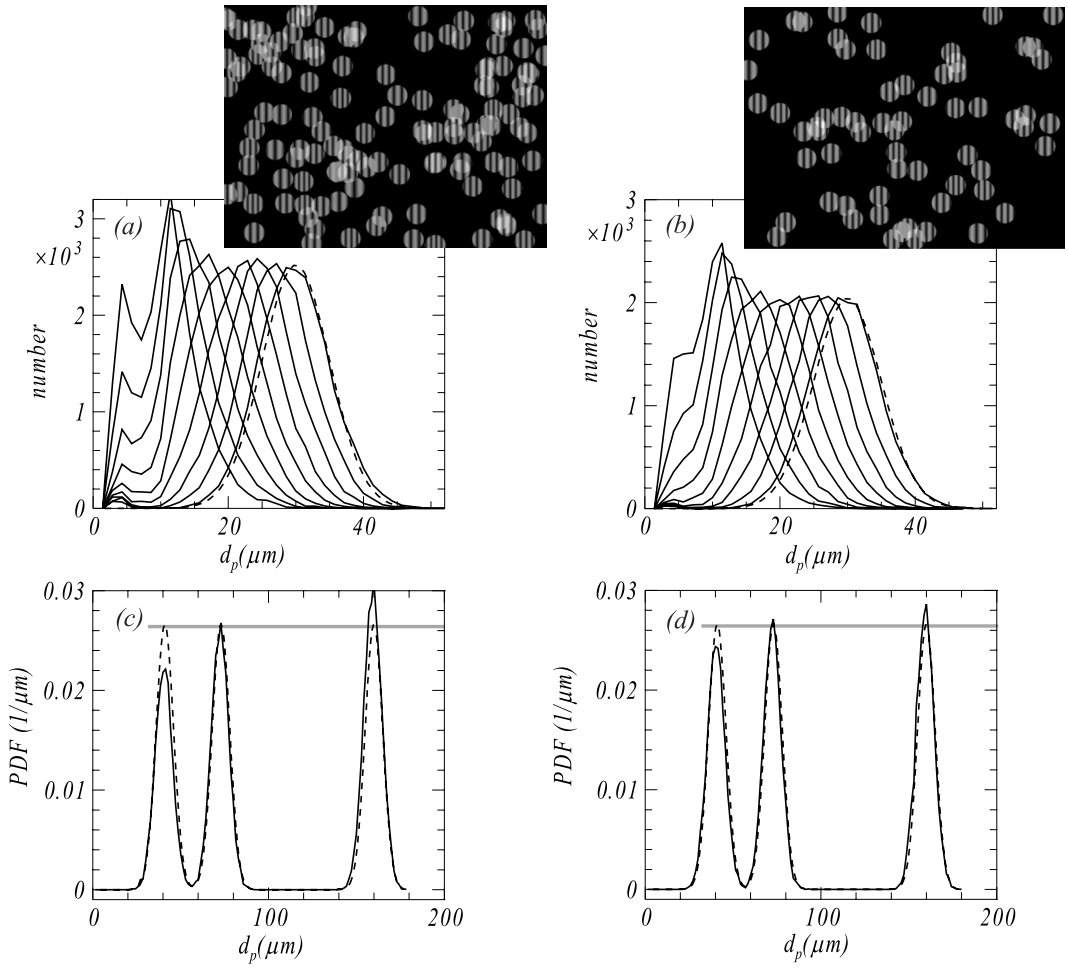

FIG. 3. (a) Particle size histogram measured from simulated images, with 128 particle images per frame, and 1024 frames. (b) Same as (a), but 64 particle images per frame. The synthetic images were generated from Gaussian particle size PDF's with mean $d_m = 10 \ldots 30\,\mu$m, in steps of 2.5 μm and Gaussian width $d_\sigma = 5\,\mu$m. For $d_m = 30\,\mu$m, it is indicated by the dashed line. The images are for the case $d_m = 30\,\mu$m. (c) Particle size distribution function measured from simulated images, with 129 particle images per frame, and 1024 frames. (d) Same as (c), but 63 particle images per frame. The synthetic images were generated from particle size PDF's consisting of 3 Gaussian peaks at $d_m = 41, 73$, and 16 μm and $d_\sigma = 5\,\mu$m; they are indicated by the dashed lines. Also shown in (d) are the results for 129 *ellipsoidal* particle images per frame with aspect ratio 1/2, but the two curves coincide. The dashed lines indicate the input PDF, the horizontal grey lines illustrate the d_p-independent peak heights of the input particle distribution. The PDF's have been normalized.

a particular particle disk. It does not identify a particle disk through its edges, not through its intensity maximum, but through its known shape—a disk or an ellipse if cylindrical lenses are involved in the imaging.

The first question is if a particle found with our methods actually corresponds to a true particle disk, or falls somewhere in between overlaps. The answer can be found in Fig. 5(a), where we show the histogram of distances of a found particle disk to the one in the simulated image that is nearest. Clearly, most particle disks are identified correctly, 94% of the found disks fall within $r_i/2$ of a simulated disk for the densest image (Fig. 3(a)). If particle disks overlap, the next question is if our method selects the brightest of a group of overlapping particle disks. The answer is in Fig. 5(b), where we show the

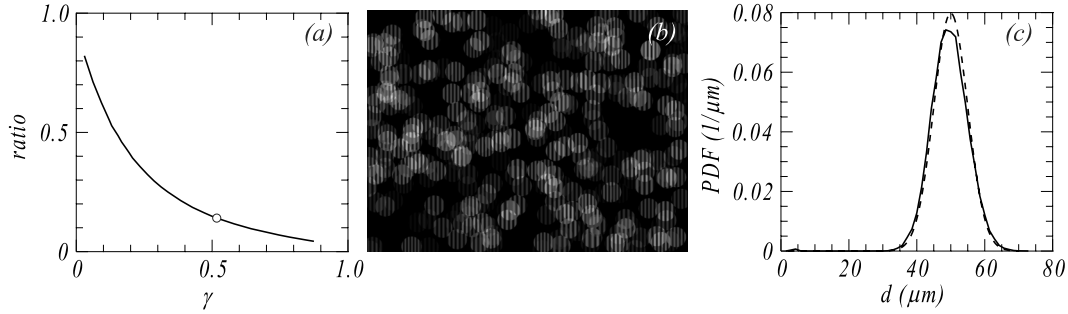

FIG. 4. (a) Fraction of found particle images as a function of the overlap coefficient γ. (b) Snapshot of particle images corresponding to the open circle in (a) ($\gamma = 0.51$). (c) Full line is the measured particle diameter PDF for $\gamma = 0.51$, the dashed line is the input-PDF. Both PDF's are normalized to one.

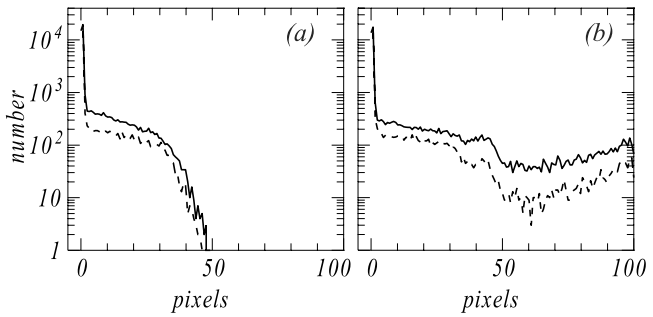

FIG. 5. (a) Histogram of distances of a found particle disk to the one in the simulated image that is nearest. The conditions are those from Fig. 3. The full line corresponds to 128 particle disks per image, the dashed line to 64 particle images. The disk radius r_i is 50 pixels. For 128 (64) particle disks per image, each found particle disk overlaps on average with 2.5 (1.6) disks in a simulated image. (b) Same as (a), but now the distance is to the brightest simulated particle disk in an overlapping cluster.

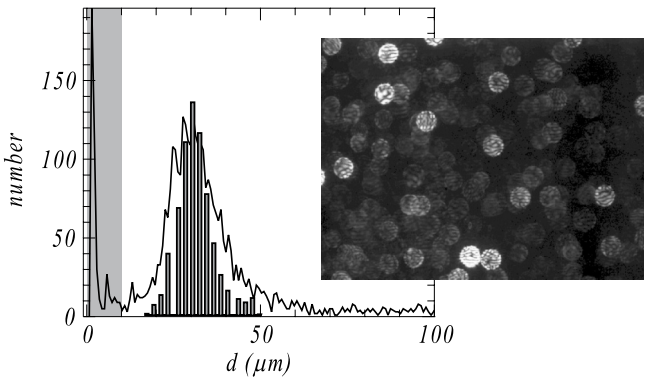

FIG. 6. Comparison of particle size distribution function measured from 1.2×10^4 calibrated glass spheres by IPI and microscopy (in grey). Inhomogeneities in the refractive index of the glass microspheres result in wavy interference patterns. In this arrangement, the fringes run horizontally. The greyed region denotes the droplet diameters that are too small to be estimated correctly because particle disks contain less than approximately one intensity minimum.

histogram of distances of a found particle disk to the original brightest one in an overlapping cluster. In most cases (83%), the brightest of a cluster corresponds to the found particle disk.

From these simulations, we conclude that our methods find the correct PDF of particle sizes, but errors arise if particle disks start to overlap severely, errors which we have quantified. These overlaps first affect small ($d_p \lesssim 15$ μm) particles with disks containing less than two fringes, and the smallest sizes of very broad particle size distributions.

As is clear from Figs. 3(c) and 3(d), overlapping particle disks with different fringe frequencies do not lead to mixture frequencies, and thus to apparent particle sizes which are a combination of the sizes of the true particles. The reason for this is the use of the Fourier transform for the initial guess of the spatial frequency and phase. In the case of partial overlap, we almost always find the disk with the largest intensity, whose spatial frequency dominates the spectrum that provides the initial guesses. Only when the disks perfectly overlap, would the spatial frequency be ambiguous.

Finally, the extension to ellipsoidal particle disks using cylindrical optics affects the results in a completely predictable manner: at a given accuracy of the measured PDF, decreasing the aspect ratio to 1/2 allows us to increase the particle density by a factor 2.

Let us again emphasize that our approach differs from all earlier work, where the main concern was the correct identification of droplets, their location, and their velocity, in addition to their size. Our interest is in the statics of the size distribution.

C. Calibrated glass spheres

After having established the functionality of our algorithm with synthetic data, we test it once again, by imaging interference patterns of soda-lime glass microspheres (refractive index $m = 1.5$; White House Scientific, Chester, England) whose diameters have been measured using a microscope. These spheres were sprinkled into a light sheet. The light source is a Nd:YAG laser (CFR 150, Quantel) with wavelength $\lambda = 532$ nm expanded into a light sheet using a cylindrical lens. We image the droplets using a 1200×1600 pixel CCD camera (ES 2020, Redlake) and a $f = 105$ mm, $d_a = 42$ mm lens, placed at an object distance $v = 0.34$ m, and scattering angle $\theta_r = 85°$.

Figure 6 compares the histograms obtained through IPI and microscopy, which are in good agreement. Solid spheres provide an attractive means of calibration, but the interference fringes are not perfect. Even though the microspheres are spherical and smooth, inhomogeneities in their refractive index produce wavy fringe patterns when imaged with the IPI setup. The IPI algorithm is robust enough to interpret the wavy fringes and reproduce the histogram of particle distributions, even though images have many particle disk overlaps. The waviness of the fringes may well be responsible for the difference between the interferometrically and directly measured PDF's.

As can be seen from the microscopy measurement, spheres greater than 50 μm are not present; nevertheless, they appear in the IPI measurement. Such sizes are artificially produced when extremely noisy images appear, and the processing algorithm cannot find a better fit. Due to this artifact, care must be taken on the quality of the images. The wavy fringes exacerbate the noise levels with respect to the signal, as they reduce the contrast between the bright and dark fringes.

III. APPLICATION TO THE SPINNING DISK AEROSOL GENERATOR

As an illustration, we will now apply our analysis methods to droplets generated by a spinning disk droplet generator. In our application, a study of the dynamics of droplets in a turbulent cloud chamber, we use droplets with mean diameter $10 \ldots 60$ μm. This mean diameter is controlled by the rotation rate of the spinning disk, and we are interested in the PDF of droplet sizes. In order to appreciate the form of these PDF's, it is necessary to briefly describe the principle of the spinning disk aerosol generator. Fluid is applied near the center of a fast spinning disk, wetting its surface completely. Due to the centrifugal force, droplets will be ejected tangentially. Their size is determined

by the angular velocity of the disk, the fluid density, and its surface tension. The principle of the spinning disk generator is well established,[12–14] but little is known about the PDF, with most literature providing only the mean value of the droplet diameter and no information about its spread (see, e.g., Ref. 14).

Depending on the flow rate of the fluid supplied to the disk surface, droplets are either ejected directly, or ligaments first form which break up into droplets. In the first mode of operation, nearly monodisperse droplets are created, trailed by much smaller droplets that result from the trailing ligament breakup. Balancing inertial and surface tension forces provides the droplet primary diameter d_p as a function of the disk radius R, its angular velocity ω, the fluid density ρ, and the surface tension σ, $d_p/R = \mathrm{We}^{-1/2}\mathrm{Qu}$, in terms of the Weber number We, or

$$d_p = \frac{\mathrm{Qu}}{(R\rho/\sigma)^{1/2}\omega}. \tag{6}$$

The number Qu depends weakly on the supply rate Q of the fluid. The analysis of many experiments lead Davies and Cheah[14] to the following empirical relation:

$$\mathrm{Qu} = \frac{1}{8}(\log \mathrm{Qe} + 2.85)^2 + 2.15. \tag{7}$$

The dimensionless flow rate, $\mathrm{Qe} = Q/(2\pi R^2(\nu\omega)^{1/2})$, is formed from Q and a reference value for a thin film driven by a centrifugal force, with ν the kinematic viscosity. Experiments show that the transition from direct droplet ejection to ligament formation occurs at $\mathrm{Li} \simeq 0.08$, with the ligament number $\mathrm{Li} = \mathrm{QeWe}^{1.15}\mathrm{Re}^{-0.95}$, which compares the length of the attached ligaments to their mutual distance.[14]

In summary, Eqs. (6) and (7) predict the average size of the droplets, while the value of the ligament number is relevant for the occurrence of satellite droplets, which is important for the shape of the PDF.

For this study, we use an air-driven spindle (EST 1000K, Mannesmann-Demag) and two disks: radii 1 and 4 cm. Both disks are manufactured in-house out of stainless steel. The maximum angular velocity reached by the spindle is approximately 3600 s^{-1} for the large disk and 7500 s^{-1} for the small one. Uniform wetting is crucial to create a uniform film. We are interested in droplet sizes between 10 μm and 60 μm. Given our maximum angular velocities, we must reduce the surface tension by means of surfactant addition in order to achieve such diameters. This also ensures proper wetting. The surface tension $\sigma = 3 \times 10^{-2}$ N/m. We used demineralized water with Triton-X100 at a 1% by volume to achieve the above surface tension. A rotating disk causes a flow normal to its rotation axis with the induced flow velocity $u \propto R\omega$. This induced flow may be problematic in experiments. For a given droplet size d_p, a disk with large radius can rotate more slowly, but the secondary flow is larger. From Eq. (6), we see that $u \propto R^{1/2}d_p^{-1}$, so that fast-rotating, small disks are preferred.

Each data set contained 1000 frames taken at a sampling rate of 15 Hz. The number of valid droplets imaged in each frame depended on the particular optical setup of each case, i.e., the values of v, f and d_a.

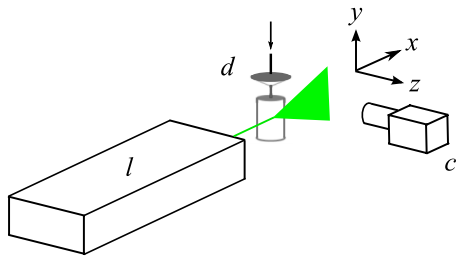

FIG. 7. Experimental setup for measuring droplet sizes from a spinning disk aerosol generator. A laser l illuminates the droplets being generated by the spinning disk d. The optical axis of the camera c is perpendicular to the laser sheet, i.e., $\theta_r = 90°$. The intensities of the reflection and first order refraction are comparable at this angle for the droplet sizes of interest. The arrow points to the needle which feeds liquid onto the disk.

Measurement of droplets with diameters in the vicinity of 30 μm presents a few practical issues. As apparent from Fig. 1, a shorter object distance v is desirable to increase the fringe frequency. Similarly, a larger aperture diameter will result in more inlying fringes. Unfortunately, these two approaches for decreasing the fringe spacing may have a negative impact on the data. To locate the particle images, our algorithm relies on the uniform diameter of the interference disks, which can only be achieved if the object distance v is equal for all droplets, that is, all imaged droplets lie on a thin sheet parallel to the image plane. Lenses with large focal length are more susceptible to variations in spot size since a small change in the object distance v has considerable impact on the image distance b. This is particularly problematic when big droplets are imaged, since they can scatter sufficient light to be detected even when outside the laser sheet (Fig. 7). To ensure that the spot diameter remains constant, a compromise between the focal length and the aperture diameter of the objective must be sought depending on the droplet size.

Figure 8 shows droplet diameter PDF's for two disk radii, $R = 1$ cm, and $R = 4$ cm, and a range of rotation speeds. The particle size distribution functions show a large peak at $d_p \approx 1.5$ μm, which corresponds to particle disks without interference fringes. These blank disks are produced by very small droplets; such images contain too little information, and our algorithm decides on a fringe spacing which equals half the droplet disk diameter. Particle disks with a single intensity minimum, which are often the result of overlaps, give rise to another parasitic peak at $d_p \approx 5$ μm or $d_p \approx 9$ μm, depending on the optical arrangement used. This parasitic peak can also be observed in Fig. 6 of the calibrated glass spheres, and in the PDF of the simulated images Fig. 3(a). Although the origin of parasitic peaks is understood well, they are still shown in the greyed regions of Figs. 8 and 6.

In Fig. 9, we summarize the results for the mean and standard deviation of the droplet distributions as a function of the rotating disk spinning rate for two disk diameters. The positions and widths of the primary peak in the PDF's were found using Gaussian fits. The length of the error bars indicates the standard deviation. For the $R = 1$ cm disk, we have repeated the experiments using a commercial particle sizer (Malvern Mastersizer). In this case, we compare the

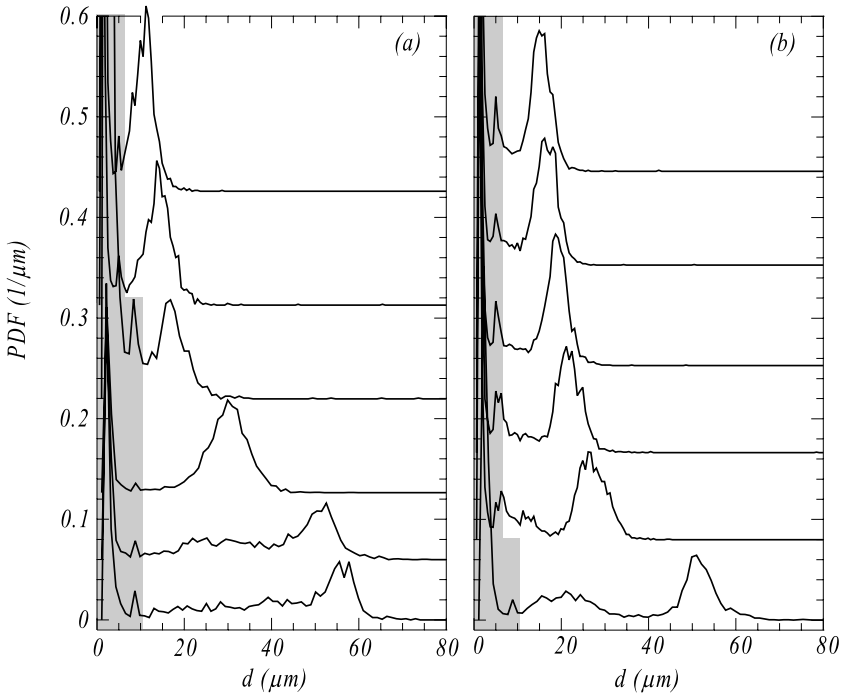

FIG. 8. Particle diameter PDF's of droplets generated by spinning disks with radius $R = 1$ and 4 cm for case (a) and (b), respectively. The rotation speed of the disk decreases from top to bottom. For frame (a), the values are $\omega = 7.6, 5.8, 5.1, 3.5, 2.2$, and $2.1\times10^3\,s^{-1}$. At $\omega = 7.6\times10^3\,s^{-1}$, the ligament number is $Li = 3\times10^{-3}$. In the case of frame (b), the rotation speeds are $\omega = 3.7, 3.6, 3.1, 2.8, 2.2$, and $1.2\times10^3\,s^{-1}$. At $\omega = 1.2\times10^3\,s^{-1}$, the ligament number is $Li = 3.5\times10^{-5}$. For large enough mean droplet diameters, the contribution of the satellite droplets can be observed as a broad distribution centered at $\approx d_p/3$ for the $R = 4$ cm disk. This distribution is much broader in case of the $R = 1$ cm disk. The greyed regions denote the droplet diameters that are too small to be estimated correctly because particle disks contain less than approximately one intensity minimum. The size of this region depends on the optical arrangement used, for the region reaching to 10 μm, a lens with 55 mm focal length was used, while a 105 mm lens was used in the region reaching to 7 μm. Particle size information inside these regions can only be obtained using a different optical arrangement.

mean and width of the droplet *volume* PDF's. For the mean droplet size, the agreement with the IPI technique described in this paper is very good. The peaks in the PDF's of the commercial particle sizer are broader due to an unavoidable coarser binning.

We also compare the mean droplet sizes to the predicted diameters from Davies and Cheah.[14] For the large disk the agreement is excellent, but the theory predicts significantly larger mean diameters for the small spinning disk.

A. Satellite droplets

For large enough mean droplet diameters, the contribution of the satellite droplets can be observed in Fig. 8 as a broad distribution centered at $\approx d_p/3$ for the $R = 4$ cm disk. This distribution is much broader in case of the $R = 1$ cm disk.

Satellite droplets are a result of ligament breakup. As a primary droplet breaks loose, smaller satellite droplets are

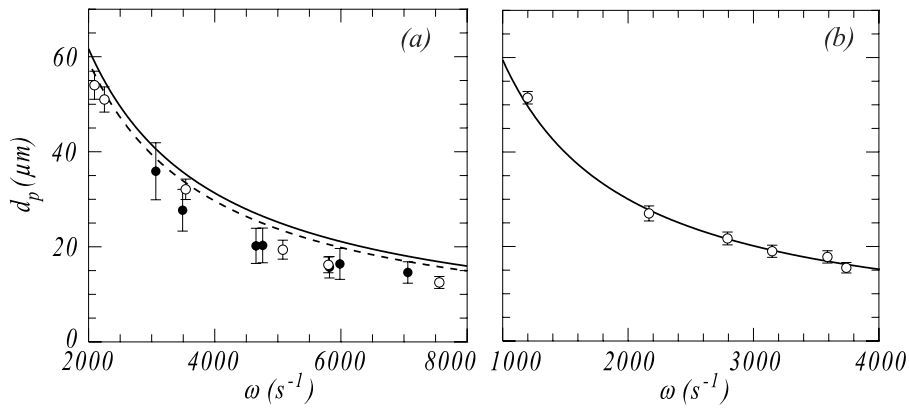

FIG. 9. Mean droplet sizes of spinning disk aerosol generator, measured using IPI and using a commercial particle sizer. Open symbols with error bars: mean diameter of primary droplets as a function of angular velocity for (a) $R = 1$ cm and (b) $R = 4$ cm. The error bars indicate the standard deviation of the droplet diameters, which was obtained from a Gaussian fit to the measured PDF's. The droplet sizes were measured using the IPI procedure described in this paper. The filled symbols in (a) are the result of a measurement with a commercial particle sizer (Malvern Mastersizer). Solid lines are the predicted diameters from Davies and Cheah.[14] The dashed line is the prediction for the commercial particle sizer, which needed a 6 times larger feed rate Q. For the small disk, the measured droplets are consistently smaller than the prediction.

formed. The size and amount of satellite droplets depends on the ligament number. In direct droplet formation (Li < 7.3×10^{-2}), the size of satellite droplets varies within the range $d_p/4$–$d_p/2$.[12] The quantity also depends on the feed rate, and for Li ≤ 3×10^{-3}, only one or two satellite droplets will be created per primary droplet.[14] In our experiments, however, we see a substantially higher amount of satellite droplets whose diameter is so small that their particle disks have no fringes. This could be explained by the creation of very small droplets that arise from the break up process as seen in Fig. 2 of Davies and Cheah,[14] where one can observe tiny droplets emerging between the expected satellites.

Another explanation for the emergence of blank droplet disks in dense sprays is multiple scattering. An interesting technique to cope with this effect has been described in Berrocal *et al.*[15]

IV. CONCLUSION

We presented a novel algorithm for obtaining the particle size probability density function from interferometric particle imaging data and tested its functionality using simulated data as well as calibrated glass spheres. Particle overlaps mainly affect the size PDF of small particles whose disks contain very few fringes and very wide particle size PDF's. With circular particle disks acceptable PDF's can still be measured for overlap coefficients $\gamma \approx 0.1$ (Figs. 3(b) and 3(d)), with larger errors for twice the particle concentration. These errors can be reduced in a predictable way using the elliptical particle disks which are imaged using cylindrical lenses.

Using this algorithm, we analyze the droplet distributions produced by a spinning disk aerosol generator. The measured mean droplet diameter compares well with the predictions of literature.[14] We find a large number of satellite droplets with diameters d_{sat}, $d_{sat} \lesssim 5$ μm, whose size could not be measured and are considerably smaller than the expected satellite droplet diameter of $d_p/4 < d_{sat} < d_p/2$. The results compare very well to those obtained from a commercial particle sizer. Unlike such an apparatus, the simple IPI setup can be integrated with an experimental setup to provide an *in situ* measurement of droplet size PDF's.

ACKNOWLEDGMENTS

This work is part of the research programme of the "Stichting voor Fundamenteel Onderzoek der Materie (FOM)," which is financially supported by the "Nederlandse Organisatie voor Wetenschappelijk Onderzoek (NWO)." This work is also supported by the COST Action MP0806.

[1]N. Damaschke, H. Nobach, and C. Tropea, Exp. Fluids **32**, 143 (2002).
[2]M. Maeda, T. Kawaguchi, and K. Hishida, Meas. Sci. Technol. **11**, 308 (2000).
[3]Y. Hardalupas, S. Sahu, A. M. K. P. Taylor, and K. Zarogoulidis, Exp. Fluids **49**, 417 (2010).
[4]A. R. Glover, S. M. Skippon, and R. D. Boyle, Appl. Opt. **34**, 8409 (1995).
[5]S. Dehaeck and J. P. A. J. Beeck, Exp. Fluids **42**, 767 (2007).
[6]A. V. Bilsky, Y. A. Lozhkin, and D. M. Markovich, Thermophys. Aeromech. **18**, 1 (2011).
[7]Q. Lü, X. Wang, T. Lü, Z. Li, and Y. Zhang, J. Opt. **16**, 045703 (2014).
[8]G. König, K. Anders, and A. Frohn, J. Aerosol Sci. **17**, 157 (1986).
[9]R. Ragucci, A. Cavaliere, and P. Massoli, Part. Part. Syst. Charact. **7**, 221 (1990).
[10]H.-E. Albrecht, M. Borys, N. Damaschke, and C. Tropea, *Laser Doppler and Phase Doppler Measurement Techniques* (Springer Verlag, Berlin, 2003).
[11]T. Kawaguchi, Y. Akasaka, and M. Maeda, Meas. Sci. Technol. **13**, 308 (2002).
[12]K. R. May, J. Appl. Phys. **20**, 932 (1949).
[13]W. H. Walton and W. C. Prewett, Proc. Phys. Soc., Sect. B **62**, 341 (1949).
[14]C. N. Davies and P. K. P. Cheah, J. Aerosol Sci. **15**, 719 (1984).
[15]E. Berrocal, E. Kristensson, M. Richter, M. Linne, and M. Aldén, Opt. Express **16**, 17870 (2008).